# A hybrid modal analysis for enclosed sound fields

Buye Xu[a] and Scott D. Sommerfeldt
*Department of Physics and Astronomy, Brigham Young University, Provo, Utah 84602*

A hybrid modal expansion that combines the free field Green's function and a modal expansion will be presented in this paper based on a review and an extension of the existing modal analysis theories for the sound field in enclosures. The enclosed sound field will be separated into the direct field and reverberant field, which have been treated together in the traditional modal analysis. Studies on a point source in rectangular enclosures show that the hybrid modal expansion converges notably faster than the traditional modal expansions, especially in the region near the source, and introduces much smaller errors with a limited number of modes. The hybrid modal expansion can be easily applied to complex sound sources if the free field responses of the sources are known. Damped boundaries are also considered in this paper, and a set of modified modal functions is introduced, which is shown to be suitable for many damped boundary conditions.
© 2010 Acoustical Society of America. [DOI: 10.1121/1.3493429]

## I. INTRODUCTION

Modal analysis (MA) has been widely used to study the low frequency response in enclosed sound fields. The fundamental idea of modal analysis is to express an acoustic field quantity as the summation of a complete set of properly weighted modal functions. The weighting factors are often called the modal amplitudes. The summation usually has an infinite number of terms; therefore MA is generally not a closed form solution. However, given that this infinite series converges, one can in practice truncate it to a finite summation and still reach the desired accuracy in the low frequency range. For high frequencies, where a very large number of modal functions must be included to achieve an acceptable accuracy, MA is less applicable.

Normal mode analysis (NMA)[1] is probably the simplest and most widely used modal analysis in the literature. It is, however, only suitable for enclosures with rigid or very lightly damped boundaries. Dowell, *et al.* developed a more comprehensive modal analysis theory, so-called classical modal analysis (CMA), which is based on the Green's divergence theorem.[2] CMA is capable of computing sound fields in damped enclosures but, as a consequence, the modal functions are coupled and the convergence speed is usually very slow.[3] NMA and CMA use the same set of eigenfunctions solved from an eigenvalue problem as the modal functions, but have different mechanisms to generate the modal amplitudes. This set of eigenfunctions is called the "normal modes" in this paper to distinguish from other sets of modal functions discussed later. The normal modes and the linear combination of them only satisfy rigid boundary conditions; therefore, large errors are often observed in the regions near damped boundaries. This issue can be understood as the Gibb's phenomenon.[4]

The eigenfunctions that satisfy the same boundary conditions as the enclosure can be solved numerically from an exact eigenvalue problem[5,6] and are called "exact modes" in this paper. The exact modes are uncoupled and automatically match the boundary conditions, which make them a very good candidate for the modal functions of modal analysis.[6] However, there are several negative properties associated with them. First of all, the completeness of this set of modal functions is always assumed without being proven. Second, the "orthogonality" relationship among these functions is abnormal, which may cause inconvenience for many applications. Finally, solving the exact eigenvalue problem involves numerical root searching in the complex domain which is complicated and time consuming. Because of these disadvantages, MA using the exact modes (exact modal analysis or EMA) is not utilized much in the literature.

In this paper, a new set of modal functions (modified modes), which partially satisfy the boundary conditions, will be introduced. Compared to the normal modes, modified modes are also coupled but can be easily simplified in many cases. Modal analysis based on the modified modes (MMA) also introduces errors on boundaries but performs better than CMA. Unlike the exact modes, modified modes are orthogonal and complete. Although a numerical root search is still required, only real values need to be considered, which greatly simplifies the searching algorithm.

In the literature related to modal analysis, distributed sources on boundaries, such as a piston source mounted on the inside surface of a room, are often considered. Point sources, though more fundamental and very important for many applications such as sound power prediction for sources inside rooms, active noise control, and so on, are not sufficiently studied, partially due to the very slow convergence rate of MA in the near field. Maa proposed a method of introducing the free field Green's function (FFGF) in addition to the MA solution for sound fields, which essentially divides the sound field into a direct field and a reverberant field.[7,8] Although his development was based on a faulty as-

---
[a]Author to whom correspondence should be addressed. Electronic mail: buye.xu@gmail.com

sumption that the classical modes are not complete, the idea of dividing the enclosure's sound field into a direct field and a reverberant field has merit. In this paper, a hybrid model that combines the free field Green's function and a modal expansion will be presented based on a rigorous mathematical derivation. Examples shown later in this paper confirm that this hybrid method not only greatly improves the convergence rate, but also provides a better way to study the physical properties of enclosed sound fields. For a complex source, the hybrid method can be easily modified by replacing the FFGF with the free field response of the source. A simple example will be given in Sec. IV C.

This paper is organized as follows. In Sec. II, the general theory of modal expansion will be reviewed; a modified modal expansion and a hybrid model will also be introduced. In Sec. III, results of different modal expansion models will be compared and discussed for both one dimensional and three dimensional cases. Further examples of implementing the hybrid modal expansion will be discussed in Sec. IV.

## II. THEORETICAL DERIVATION

Inside an enclosure, the sound pressure field excited by a point source satisfies the wave equation

$$\nabla^2 p - \frac{1}{c^2}\frac{\partial^2 p}{\partial t^2} = -Q_0(t)\delta(r - r_o), \tag{1}$$

where $p$ is the sound pressure, $c$ represents the acoustic phase speed, and $Q_0(t)\delta(r - r_o)$ represents the point source.

Taking the Fourier transform of both sides of Eq. (1), it becomes the non-homogeneous Helmholtz equation:

$$\nabla^2 \hat{p} + k_0^2 \hat{p} = -\hat{Q}_0(\omega_0)\delta(r - r_o), \tag{2}$$

where $\hat{}$ indicates a frequency domain quantity, $\omega_0$ is the excitation frequency, and $k_0$ is the acoustic wave number.

The boundary condition is usually assumed locally reacting and given as follows:

$$\frac{\partial \hat{p}}{\partial n}/\hat{p}|_S = \beta = -ik_0\frac{\rho_0 c}{z}, \tag{3}$$

where $\rho_0$ is the air density, $z$ is the specific acoustic impedance of the boundary, and $\beta$ is the normalized specific acoustic admittance. Note that this $\beta$ differs from the standard definition of the specific acoustic admittance by the constant $-ik_0\rho_0 c$, which is a pure imaginary number.

The solution, $\hat{p}$, can be expressed as a linear combination of modal functions, $\psi_n$,

$$\hat{p} = \sum_{n=1}^{N} q_n\psi_n, \tag{4}$$

where the modal amplitude, $q_n$, can be complex and $N$ is the total number of modal functions. (These modal functions are spatially dependent, i.e., $\psi_n = \psi_n(\vec{r})$, but for notational simplicity the spatial dependence is omitted here.) From Euler's equation, one can easily obtain the modal expression for particle velocity (assuming $e^{i\omega t}$ time dependence),

$$\hat{v} = -\frac{1}{i\omega\rho}\sum_{n=1}^{N} q_n \nabla \psi_n. \tag{5}$$

A frequent choice for $\psi_n$ is the eigenfunctions of the following eigenvalue problem:

$$\nabla^2\psi_n = \lambda_n\psi_n = -k_n^2\psi_n, \tag{6a}$$

$$\frac{\partial \psi_n}{\partial n}/\psi_n|_S = \beta', \tag{6b}$$

where $\lambda_n$ denotes the eigenvalue, and $\beta'$ could be any value of choice. If $\beta'$ is real, however, the eigenvalues are real and the resulting modal functions are guaranteed to be complete and orthogonal.[9] Orthogonality implies $C_{mn} = \iiint_V \psi_m^*\psi_n d^3x = \Lambda_{mn}\delta_{mn}$, where $\delta_{mn}$ is the Kronecker delta function, and $\Lambda_{mn}$ is a normalization constant. The eigenvalues are often assumed non-positive, and thus written as $-k_n^2$ as shown in Eq. (6a), but they could be positive if $\beta' < 0$ for some or all of the boundary.

To solve for $q_n$, the Green's theorem can be applied as follows:

$$\int\int\int_V (\psi_m^*\nabla^2\hat{p} - \hat{p}\nabla^2\psi_m^*)d^3x = \oint_S \left(\psi_m^*\frac{\partial \hat{p}}{\partial \mathbf{n}} - \hat{p}\frac{\partial \psi_m^*}{\partial \mathbf{n}}\right)da, \tag{7}$$

where the volume integral covers the entire volume inside the enclosure, and the surface integral is evaluated on the entire inside surface of the enclosure. Substitution of Eqs. (2), (3), and (5) into Eq. (7) gives

$$\int\int\int_V [-\hat{Q}_0\delta(r - r_0)\psi_m^* - k_o^2\hat{p}\psi_m^* + k_m^2\hat{p}\psi_m^*]d^3x = \oint_S (\beta - \beta')\hat{p}\psi_m^* da$$

$$\Rightarrow \int\int\int_V (k_0^2 - k_m^2)\hat{p}\psi_m^* d^3x + \oint_S (\beta - \beta')\hat{p}\psi_m^* da = -\hat{Q}_0\psi_m^*(r_o)$$

$$\Rightarrow \sum_n (k_0^2 - k_m^2)C_{mn}q_n + \sum_n D_{mn}q_n = -\hat{Q}_0\psi_m^*(r_o)$$

$$\Rightarrow \sum_n [(k_0^2 - k_m^2)C_{mn} + D_{mn}]q_n = -\hat{Q}_0\psi_m^*(r_o), \tag{8}$$

where $D_{mn}=\oint_S(\beta-\beta')\psi_m^*\psi_n da$. Thus, $q_n$ can be solved from this linear equation group, which can also be written in matrix form as

$$\begin{bmatrix} (k_0^2-k_1^2)C_{11}+D_{11} & D_{12} & \cdots \\ D_{21} & (k_0^2-k_2^2)C_{22}+D_{22} & \cdots \\ \vdots & \vdots & \ddots \end{bmatrix} \cdot \begin{bmatrix} q_1 \\ q_2 \\ \vdots \end{bmatrix}$$

$$= \begin{bmatrix} -\hat{Q}_0\psi_1^*(\boldsymbol{r_o}) \\ -\hat{Q}_0\psi_2^*(\boldsymbol{r_o}) \\ \vdots \end{bmatrix},$$

$$A \cdot Q = B, \qquad\qquad (9)$$

where $A_{mn}=(k_0^2-k_m^2)C_{mn}+D_{mn}$, $Q_n=q_n$, and $B_m=-\hat{Q}_0\psi_m^*(\boldsymbol{r_o})$

As mentioned at the beginning of this paper, the number, $N$, of modal functions is usually infinity. Moreover, matrix $A$ is, though often sparse and Hermitian, nondiagonal. Therefore, the $q_n$'s are coupled and it is impossible to obtain an exact solution.

In practice, however, if $q_n$ goes to zero quickly enough as $n$ goes to infinity, it is possible to keep only a finite number of $\psi_n$'s as well as $q_n$'s and obtain a desired accuracy.

Results that have been developed can be applied to enclosures of any shape. However, this paper will only focus on rectangular shapes. In particular, the dimensions of the rectangular enclosure are $L_x \times L_y \times L_z$ and one of the corners sits at the origin with the three adjoint edges lying along the positive direction of the $X$, $Y$ and $Z$ axes. In addition, it is assumed that the specific acoustic admittance, $\beta$, is constant for each of the boundaries, and is denoted by $\beta_{x0}$, $\beta_{xL}$, $\beta_{y0}$, $\beta_{yL}$, $\beta_{z0}$ and $\beta_{zL}$, where $\beta_{x0}$ stands for $\beta$ at $x=0$, $\beta_{xL}$ stands for $\beta$ at $x=L_x$, and so forth.

### A. Classical modal analysis

For classical modal analysis, $\beta'$ in Eq. (6b) is set to be zero. Therefore, the eigenfunctions (normal modes) and eigenvalues can be solved easily for rectangular enclosures,

$$\psi_n = \psi_{lmo} = \cos(k_{xl}x)\cos(k_{ym}y)\cos(k_{zo}z), \qquad (10a)$$

$$k_{xl}=\frac{l\pi}{L_x}, \quad k_{ym}=\frac{m\pi}{L_y}, \quad k_{zo}=\frac{o\pi}{L_z},$$

$$k_n^2=k_{xl}^2+k_{ym}^2+k_{zo}^2, \qquad\qquad (10b)$$

where $l$, $m$ and $o$ are nonnegative integers.

This set of normal modes is complete and orthogonal because $\beta'$ is real, but it is always infinite and usually coupled for non-rigid boundaries. The hope here is that $q_n$ converges to zero quickly so that truncations can be made. Moreover, if the damping is small, or more precisely $\beta-\beta' \ll 1$, $A_{mn}$ can be "uncoupled" by setting nonzero off-diagonal terms to zero to simplify the computation.[2] Studies on one-dimensional (1-D) sound fields in ducts show that when damping is added to the system the coupled model has to be considered and many more iterations are needed.[3,10] Ref. 10

also points out that even if a large number of terms are included the coupled model still converges poorly for the acoustic intensity.

The classical modal analysis converges slowly not only for the acoustic intensity but also for sound pressure as well as particle velocity, especially in the spatial region close to the boundaries.

### B. Modified modal function

In order to reduce the effects of off-diagonal terms in the matrix $A$ in Eq. (9), yet keep $\beta'$ real, a good choice for $\beta'$ is the real part of $\beta$. The modified modes thus can be solved for from Eq. (5), and have the form

$$\psi_n = \psi_{lmo} = \left[\cos(k_{xl}x)-\frac{\beta'_{x0}}{k_{xl}}\sin(k_{xl}x)\right]\cdot\left[\cos(k_{ym}y)\right.$$
$$\left.-\frac{\beta'_{y0}}{k_{ym}}\sin(k_{ym}y)\right]\cdot\left[\cos(k_{zo}z)-\frac{\beta'_{z0}}{k_{zo}}\sin(k_{zo}z)\right], \quad (11)$$

where $k_{xl}$, $k_{ym}$ and $k_{zo}$ can be solved from the following equations:

$$\tan(k_{xl}\cdot L_x)=\frac{(\beta'_{x0}+\beta'_{xL})k_{xl}}{\beta'_{x0}\cdot\beta'_{xL}-k_{xl}^2},$$

$$\tan(k_{ym}\cdot L_y)=\frac{(\beta'_{y0}+\beta'_{yL})k_{ym}}{\beta'_{y0}\cdot\beta'_{ym}-k_{ym}^2},$$

$$\tan(k_{zo}\cdot L_z)=\frac{(\beta'_{z0}+\beta'_{zL})k_{zo}}{\beta'_{z0}\cdot\beta'_{zL}-k_{zo}^2}. \qquad (12)$$

The general derivation carried out at the beginning of Sec. II [Eqs. (4), (5), (6a), (6b), and (7)–(9)] is also applicable for modal analysis based on this new set of modal functions.

Generally, the values of $k_{xl}$, $k_{ym}$ and $k_{zo}$ in Eqs. (12) cannot be solved analytically, and thus a numerical method is needed. Because $\beta'$ is real, these modified modes are complete and orthogonal. The eigenvalues, $\lambda_n=-k_n^2$, are real, but they could be positive for stiffness like boundary conditions. Therefore, $k_{xl}$, $k_{ym}$ and $k_{zo}$ could be pure imaginary numbers.

$A$ is still not a diagonal matrix, since $D_{mn}\neq 0$. However, unlike normal modes, this new set of modal functions do not reach maxima on the boundary and, in addition, the value of $\beta'$ also reduces the value of $\beta-\beta'$ which can be found in the expression for $D_{mn}$. This implies a reduced effect of the off-diagonal terms, $D_{mn}$ in $A$.

Because the boundary condition is partially satisfied, the modified modal analysis is expected to perform better than normal modal analysis.

### C. Hybrid modal analysis

Due to the singular nature of a point source, all the modal models discussed above converge very slowly at field points close to a point source. In order to overcome this problem, a free field Green's function is introduced to the solution of Eq. (2):

$$\hat{p}(\boldsymbol{r}) = G(\boldsymbol{r}|\boldsymbol{r_o}) + F(\boldsymbol{r}), \qquad (13)$$

where $G(\boldsymbol{r}|\boldsymbol{r_o})$ represents the pressure field associated with the free-field Green's function that satisfies Eq. (2) by itself, and $F(\boldsymbol{r})$ is a solution of the homogenous Helmholtz equation. $G(\boldsymbol{r}|\boldsymbol{r_o})$ can be expressed as

$$G(\boldsymbol{r}|\boldsymbol{r_0}) = \frac{\hat{Q}_0(\omega_o)}{4\pi|\boldsymbol{r} - \boldsymbol{r}_o|} e^{-i k_o \cdot (\boldsymbol{r} - \boldsymbol{r}_o)}, \qquad (14)$$

where $\boldsymbol{r}_o$ designates the location of the point source.

From the point of view of room acoustics, the sound field is now divided into a direct field, $G(\boldsymbol{r}|\boldsymbol{r_0})$, and a reverberant field, $F(\boldsymbol{r})$. For the near field, the direct field dominates; at large distances, the direct field decays at a rate proportional to $1/|\boldsymbol{r} - \boldsymbol{r}_o|$, and, eventually, beyond a certain distance the reverberant field becomes stronger than the direct field. Note that neither $G(\boldsymbol{r}|\boldsymbol{r}_o)$ or $F(\boldsymbol{r})$ satisfies the boundary condition represented by Eq. (3), but together they can potentially be constructed to do so.

$F(\boldsymbol{r})$ can be solved in terms of modal expansions, and any modal functions can be used. However, on one hand, because the reverberant field usually dominates on the boundaries, a modal function set that can better match the boundary condition is desired; on the other hand, the exact modes may not be the best candidate since, in addition to the issue of completeness and orthogonality, $F(\boldsymbol{r})$ should not satisfy the boundary condition by itself. Therefore, the modified modes are expected to be a desirable candidate. The mode amplitudes, $q_n$, can be solved by a means that is very similar to the development carried out before. The only difference is that the right hand side of Eq. (8) is modified and the new equation reads

$$\sum_n [(k_0^2 - k_m^2)C_{mn} + D_{mn}]q_n = -\oint_S \psi_m^* \left( \beta G - \frac{\partial G}{\partial \mathbf{n}} \right) da. \qquad (15)$$

Consequently, the B matrix in Eq. (9) is modified to $B_m = -\oint_S \psi_m^*(\beta G - \partial G/\partial \mathbf{n})da$. Note that $B_m$ now involves a surface integral which may not be easy to evaluate analytically, but a numerical evaluation is generally straightforward. By recognizing the spherical spreading nature of $G$ and $\partial G/\partial \mathbf{n}$ one can mesh the surface $S$ accordingly to make the computation more efficient.

## III. COMPARISONS

### A. Normal modes vs. modified modes in one-dimensional (1-D) cases

The sound wave inside a 1-D plane wave duct has been covered extensively by many authors.[11-13] The exact closed form solution for this problem provides a benchmark with which modal analysis results can be compared.[3,10,14]

Assume that the 1-D duct has a length, L, and that, for simplicity, two terminations are made of the same material with the specific acoustic impedance, $z$. A point source driven at frequency $f_0$ is located inside the duct at $x_o$. The governing equation for this problem is

$$\frac{d^2\hat{p}}{dx^2} + k_0^2 \hat{p} = -\hat{Q}_0 \delta(x - x_0). \qquad (16)$$

The exact plane wave solution for the sound pressure can be written as

$$\hat{p}_{exact} = -\hat{Q}_0(A \cos k_0 x + B \sin k_0 x), \qquad (17)$$

where

$$A = \begin{cases} \dfrac{k_0 \cos[k_0(L - x_0)] - \beta \sin[k_0(L - x_0)]}{2k_0\beta \cos k_0 L + (k_0^2 - \beta^2)\sin k_0 L} & \text{if } x < x_0, \\[3mm] \dfrac{(k_0 - \beta \tan k_0 L)(k_0 \cos k_0 x_0 - \beta \sin k_0 x_0)}{k_0[2k_0\beta + (k_0^2 - \beta^2)\tan k_0 L]} & \text{if } x > x_0, \end{cases}$$

$$B = \begin{cases} -A \cdot \dfrac{\beta}{k_0} & \text{if } x < x_0, \\[3mm] A \cdot \dfrac{\beta \cos(k_0 L) + k_0 \sin(k_0 L)}{k_0 \cos(k_0 L) - \beta \sin(k_0 L)} & \text{if } x > x_0 \end{cases}$$

and $\beta$ can be found in Eq. (3). The exact solution for the particle velocity can be solved from Euler's equation, and reads

$$\hat{v}_{exact} = \frac{-i\hat{Q}_0}{\rho_0 c}(A \sin k_0 x - B \cos k_0 x). \qquad (18)$$

The modal expansion solution of Eq. (16) can be solved for from Eqs. (4), (5), (6a), (6b), and (7)–(9) and reads

$$\hat{p}_{modal} = \sum_{n=1}^{N} q_n \psi_n. \qquad (19)$$

For modal function sets studied in Sec. II, $k_n$ can be solved from Eq. (12), which can be simplified to the following equations for the 1-D plane wave duct:

$$k_n \tan\left(\frac{k_n L}{2}\right) = -\beta', \qquad (20a)$$

$$\text{or } k_n \cot\left(\frac{k_n L}{2}\right) = \beta'. \qquad (20b)$$

Note that each equation above by itself only provides half of the solution set for $k_n$, but the latter equation, Eq. (20b), is found missing in some of the literature.[1,6,11] The roots of these two equations could be imaginary numbers if the boundaries are represented by a stiffness. However, for this case there should be no more than one imaginary root for each of these equations. For these roots, one can simply replace the trigonometric functions in Eqs. (19) by the corresponding hyperbolic functions to maintain the root search in the real domain.

The error associated with modal expansion solutions can be indicated by a single value:

TABLE I. 1-D ducts for comparing modal models.

|  | $z$[a] | $\alpha$[b] |
|---|---|---|
| Lightly damped duct | $50+50i$ | 0.04 |
| Damped duct 1 | $7-4.8i$ | 0.32 |
| Damped duct 2 | $2+4i$ | 0.32 |

[a]Normalized by $\rho_o c$.
[b]Normal-incidence absorption coefficient.

$$Error_p = \sqrt{\frac{\int_0^L |\hat{p}_{modal} - \hat{p}_{exact}|^2 dx}{\int_0^L |\hat{p}_{exact}|^2 dx}}. \qquad (21)$$

Although only the sound pressure is shown in Eq. (21), errors for other quantities, e.g., particle velocity, acoustic intensity, squared pressure and so forth, can also be calculated in a similar fashion.

Three specific examples will be discussed here to compare modal expansion results. In these examples, $L$, $x_0$ and $f_0$ are unchanged and have values of 2 m, 0.6 m and 500 Hz respectively. The specific acoustic impedance of the duct ends, however, varies as shown in Table I. Damped duct "1" and "2" have the same normal-incidence absorption coefficient but different phase angles for $z$.

Figure 1 compares coupled CMA and MMA. Both models work very well and converge to the exact solutions quickly. As the damping increases, especially when the phase angle of the specific acoustic impedance is greater than $\pi/4$, MMA starts to exhibit a notable faster convergence speed for sound pressure, and is thus more accurate with even a smaller number of modes. For particle velocity, MMA is only slightly better than CMA in terms of prediction errors. Additional studies show that the convergence speed of both MMA and CMA is slow at the source location. Moreover,

errors cannot be eliminated for the particle velocity on the boundaries, but MMA has constantly much less error than CMA.

To compare the "uncoupled" models [the off diagonal terms of matrix $A$ in Eq. (9) are simply set to zero], errors for squared pressure and squared particle velocity are computed instead of complex quantities because both models tend to introduce large errors in phase. As shown in Fig. 2, MMA is up to ten times more accurate than CMA for both squared quantities. It needs to be pointed out that, unlike the coupled models, the "uncoupled" models do not converge to the exact solution even in terms of amplitude, and, instead, reach an error level that cannot be reduced with additional modes, although the error using MMA is likely to be acceptable on a logarithmic scale. Figure 3 compares the "uncoupled" model predictions for the sound pressure level and particle velocity level to the exact solutions. For the case of damped duct 2, errors introduced by "uncoupled" MMA are generally acceptably small (within 0.2 dB except for the nodal points and source location) while large errors are observed with the "uncoupled" CMA. Although MMA dose not predict the correct value at nodal points, it does predict the locations of nodes correctly. Both "uncoupled" models, however, have large errors when computing the acoustic intensity (not shown in this paper), which is the result of significant phase errors for both "uncoupled" models.

Finally, it is worthwhile to take a look at the values of $\beta$ for the three boundary conditions and the corresponding values of $\beta'$ used in MMA. At 500 Hz, $\beta$ can be calculated using Eq. (3). The values are $-0.09-0.09i$, $0.61-0.89i$ and $-1.83-0.92i$ for the lightly damped duct, damped duct "1" and damped duct "2," respectively. MMA uses the real part of $\beta$ for $\beta'$ and CMA always uses zero. For the coupled models, both CMA and MMA perform well for the lightly damped duct because the value of $\beta$ is small, which leads to a small difference between $\beta$ and $\beta'$ for both modal models. As the modulus of $\beta$ increases, CMA tends to converge more
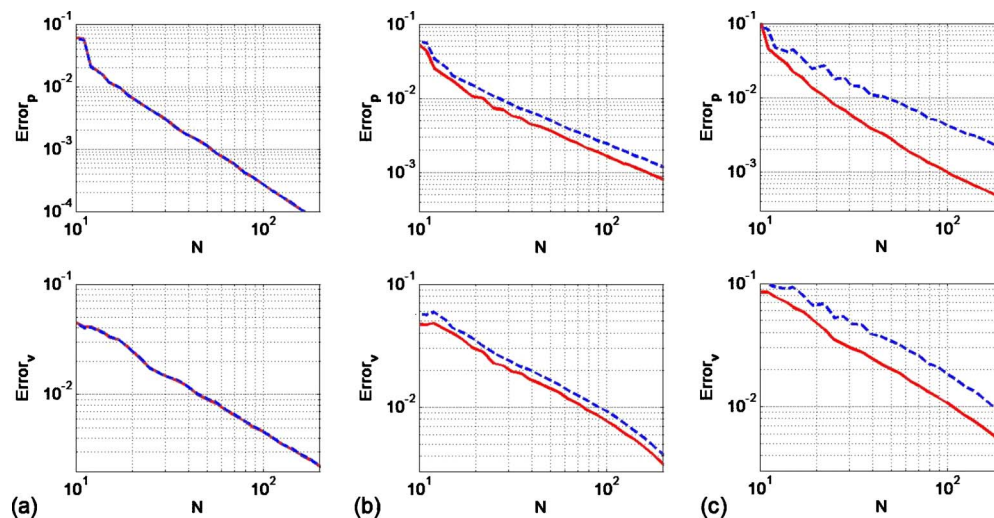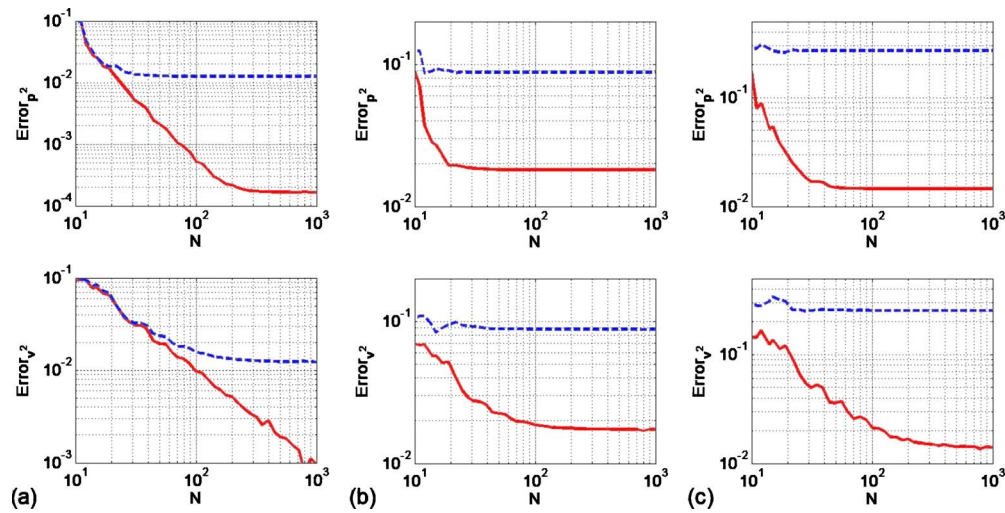


FIG. 1. (Color online) Accuracy test for the coupled modal expansions in 1-D ducts at 500 Hz [(a) lightly damped duct, (b) damped duct 1, and (c) damped duct 2]. The errors in predicting the complex pressure field and the complex particle velocity field are plotted as functions of the number of modes. Equation (21) is evaluated, but regions within 0.1 m from the point source and 0.005 m from the boundaries are excluded when evaluating the integrals. "—:" MMA; "– –:" CMA.

FIG. 2. (Color online) Accuracy test for the "uncoupled" modal expansions in 1-D ducts at 500 Hz [(a) lightly damped duct, (b) damped duct 1, and (c) damped duct 2]. The errors in predicting the squared pressure field and the squared particle velocity field are plotted as functions of the number of modes. Equation (21) is evaluated, but regions within 0.1 m from the point source and 0.005 m from the boundaries are excluded when evaluating the integrals. "—:" MMA; "− −:" CMA.

slowly. The convergence rate of MMA, however, depends not only on the modulus of $\beta$ but also on the phase. For example, $\beta$ for the damped duct "2" is larger than that for the damped duct "1"; therefore CMA performs worse for the damped duct "2". However, that is not the case for MMA, which is due to the fact that the real part of $\beta$ is larger than the imaginary part for the damped duct "2", while the opposite is true for the damped duct "1". When it comes to the "uncoupled" models, a similar trend can be observed, except that the difference between MMA and CMA is more clear. Even for the lightly damped duct, there is a notable difference between the results of CMA and MMA.

## B. Comparisons in three-dimensional cases

For three-dimensional (3-D) enclosed sound fields, the closed form solution usually does not exist, so there is not a simple benchmark to compare with. However, since both classical modes and modified modes are complete and the coupled modal expansions should converge absolutely for the entire enclosed volume except at boundaries and source

locations, a coupled modal expansion result can be accurate enough to be the benchmark if enough modes are included.

Convergence tests were carried out to compare four coupled models: CMA, MMA, GCMA and GMMA, where GCMA refers to the hybrid model using CMA and GMMA refers to the hybrid model using MMA. Sound fields in three different rectangular enclosures were computed and compared. The enclosures have the same dimensions ($e \times \pi \times 2$ m$^3$) but, as shown in Table II, different specific impedances for the boundaries. A point source was randomly chosen to be located at (1.09 m, 1.20 m, 0.7 m), and the driving frequency is 400 Hz.

Figure 4 compares the values of $\sum_{n=0}^{N} |q_n|^2$ and $\sum_{n=0}^{N} |q_n k_n|^2 / k_0^2$ that are computed from four "coupled" models. The hybrid models converge notably faster than pure modal models. MMA and GMMA converge faster than CMA and GCMA respectively. The difference in terms of the limit values between the hybrid model results and pure modal model results is due to the fact that hybrid models treat the direct sound field and reverberant field separately but the pure modal models consider them together.
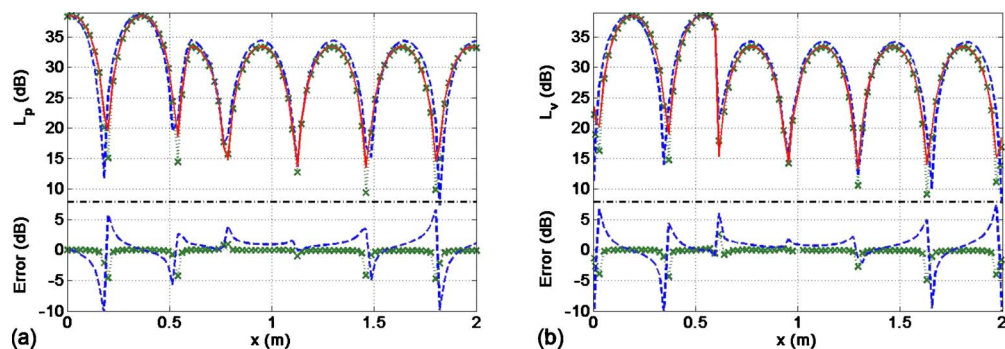


FIG. 3. (Color online) (a) Sound pressure level and (b) particle velocity level computed by "uncoupled" modal expansion models compared with the exact solution at 500 Hz in the damped duct 2 ($z = 2 + 4i$). 200 modes are included in each model. In each plot, curves above the dash dot line represent sound pressure level or particle velocity level. Curves below the dash dot line plot the errors of two modal models. "—:" exact solution; "·· × ··:" MMA; "− −:" CMA.

B. Xu and S. D. Sommerfeldt: A hybrid model analysis

TABLE II. Rectangular enclosures used for convergence test.

| | $z$ [a] | $\alpha_s$ [b] | $F_s$ [c] |
|---|---|---|---|
| Lightly damped | $200+340i$ | 0.01 | 1290 |
| Damped enclosure 1 | $10+5.5i$ | 0.4 | 190 |
| Damped enclosure 2 | $1+2.9i$ | 0.4 | 190 |

[a]Normalized by $\rho_o c$.
[b]Sabine's absorption coefficient calculated from $z$ (see Ref. 1).
[c]Schroeder frequency (Hz).

Since the GMMA model shows the fastest convergence speed in all the cases, the results computed by this model ($2 \times 10^4$ modes included) will be considered as the benchmarks to which other models can be compared. The errors of models can be calculated by Eq. (21) with $\hat{p}_{exact}$ being replaced by the benchmark value and the linear integrals being replaced by volume integrals that cover the whole interior of an enclosure. Figure 5 plots the errors for squared pressure and squared particle velocity versus the number of modes included in the coupled models. In general, the errors decrease as the number of modes increases for all the coupled models. However, the hybrid models converge much faster and thus have much less error than the pure modal models with a limited number of modes. In addition, GMMA shows obvious advantages over GCMA for the damped boundary conditions where the specific acoustic impedance of the boundary has a large phase angle.

The slow convergence speed of the pure modal models, especially for the particle velocity, is largely due to the singularity at the point source location. Averaged errors in the region that is at least 0.3 m away from the point source have also been computed. The convergence speed and accuracy of the pure modal models improve greatly, but are still notably worse than that of the hybrid models (Fig. 6).

Figure 7 compares the errors for the "uncoupled" models. Again the hybrid models work much better than the pure modal models. However, unlike the coupled models, "uncoupled" GMMA and GCMA reach an error level quickly and tend to stay at that level. Errors of the pure modal mod-

els decrease very slowly as the number of modes increases. GMMA exhibits notably better accuracy than other models. For the damped enclosures ($\alpha_s=0.4$), the averaged error is around 10 percent.

Above all, the coupled hybrid models converge notably faster and have much better accuracy than the other models when a limited number of modes are included. The difference between the GMMA and GCMA models can be either minor ("lightly damped" and "damped 1") or relatively large ("damped 2") depending on the boundary conditions, but given that GMMA usually requires more computational resources (CPU time and memory), GCMA is probably more desirable in practice. For "uncoupled" models, the pure modal models can introduce significant errors even if the enclosure is lightly damped, but the hybrid models can improve the accuracy greatly. Since there is no notable difference between "uncoupled" GMMA and GCMA in terms of computational resource requirements, GMMA is always preferred due to the better accuracy.

## IV. EXAMPLES OF USING THE HYBRID MODAL ANALYSIS

### A. Sound power

The sound power for a source inside an enclosure can be computed by integrating the acoustic intensity over a Gaussian surface inside the enclosure, where a Gaussian surface is defined as a closed three-dimensional surface through which a flux of the field is to be calculated. In this example, a rectangular enclosure (dimensions: $e \times \pi \times 4$ m$^3$, $z=(0.5+1i)\rho_0 c$, $\alpha_s=0.76$) will be considered, and the point source randomly located at (1.09, 1.04, 1.12) is driven at 495 Hz. The Gaussian surfaces are rectangular shapes with each side being parallel and equal distance, $d$, to the nearest boundary of the enclosure. Figure 8 compares the sound power results computed by coupled GMMA and CMA (1400 modes are used). The $x$ axis represents the distance between the Gaussian surface and the enclosure boundary. When $d>1.04$ the Gaussian surface begins to exclude the point source; there-
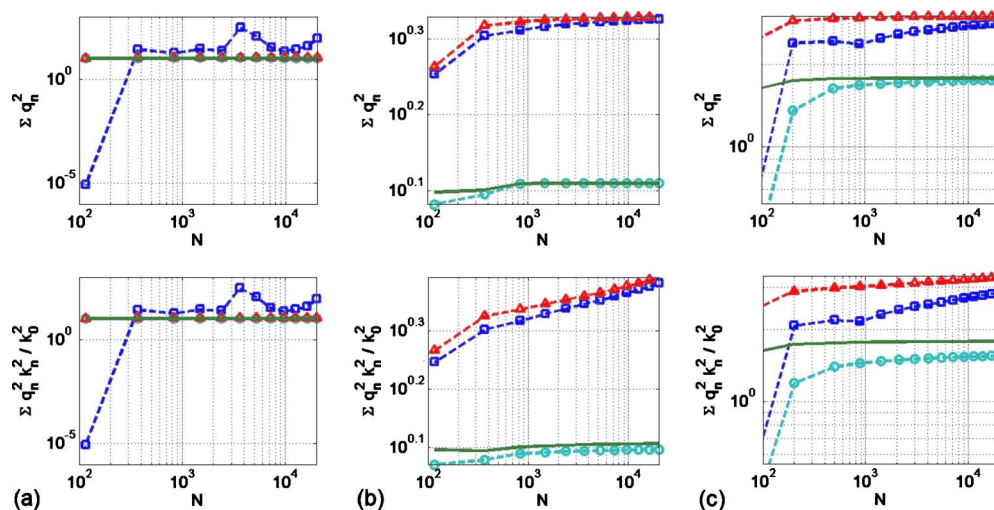


FIG. 4. (Color online) Convergence speed of the coupled modal expansion models for enclosures with different boundary conditions [(a) lightly damped, (b) damped 1, and (c) damped 2] at 400 Hz. "–□–:" CMA; "–○–:" GCMA; "–△–:" MMA; "—:" GMMA.
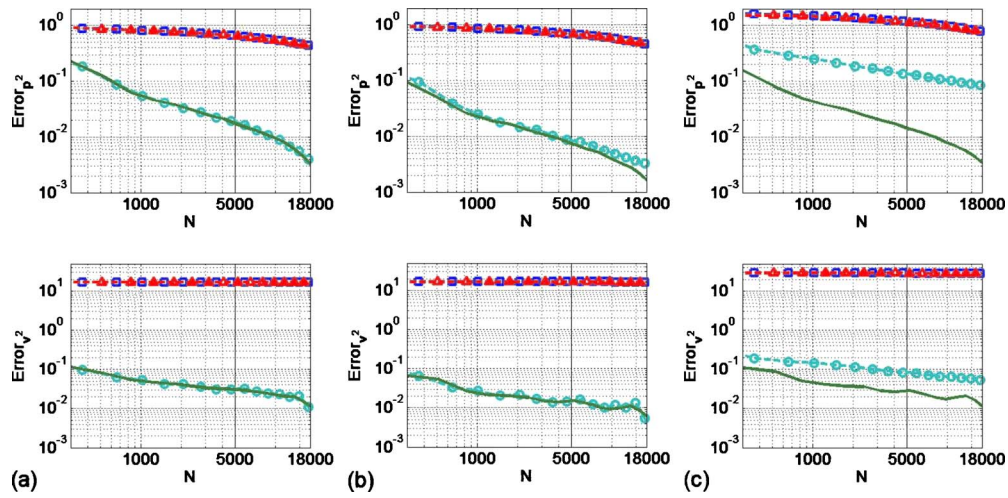
FIG. 5. (Color online) Accuracy test for the coupled modal expansion models in enclosures [(a) lightly damped, (b) damped 1, and (c) damped 2] at 400 Hz. The errors in predicting the squared pressure field and the squared particle velocity field are plotted as functions of N, the number of modes. "–□–:" CMA; "–○–:" GCMA; "–△–:" MMA; "—:" GMMA.
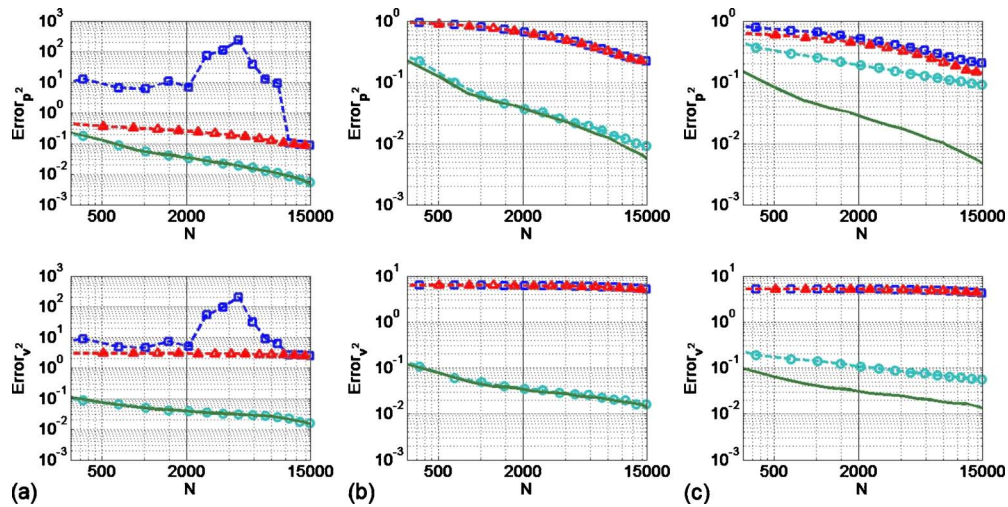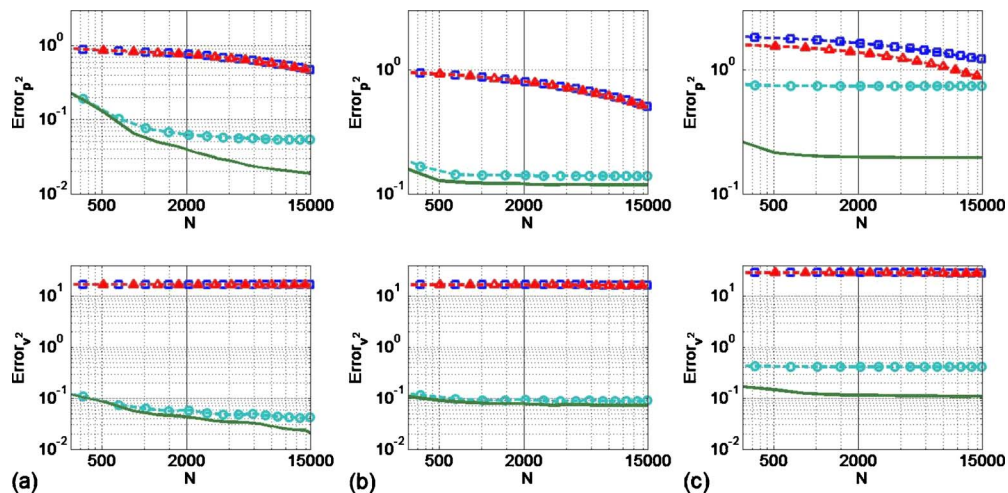


FIG. 6. (Color online) Errors of the coupled models when the near field region is excluded. The errors for the squared pressure field and the squared particle velocity field in three enclosures [(a) lightly damped, (b) damped 1, and (c) damped 2] are calculated as functions of the number of modes at 400 Hz. "–□–:" CMA; "–○–:" GCMA; "–△–:" MMA; "—:" GMMA.



FIG. 7. (Color online) Accuracy test for the "uncoupled" modal expansion models in enclosures [(a) lightly damped, (b) damped 1, and (c) damped 2] at 400 Hz. The errors in predicting the squared pressure field and the squared particle velocity field are plotted as functions of N, the number of modes. "–□–:" CMA; "–○–:" GCMA; "–△–:" MMA; "—:" GMMA.
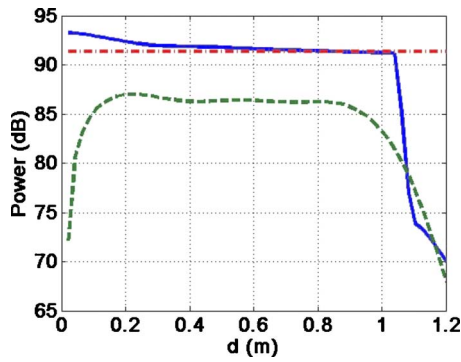
FIG. 8. (Color online) Sound power of an enclosed sound field computed by coupled GMMA and CMA at 495 Hz. The enclosed sound field is excited by a pure tone point source in a damped rectangular enclosure. The sound power results were obtained by integrating the acoustic intensity over multiple Gaussian surfaces which are rectangular shapes with each side being parallel and equal distance ($d$) to the nearest boundary of the enclosure. "—:" GMMA prediction; "– –:" CMA prediction; "–·–:" free field source power.

fore the sound power is expected to be zero. GMMA captures this sharp change very well. In addition, since the driving frequency is above the Schroeder frequency of the enclosure (111 Hz), the sound power emitted from the point source in the enclosure should be approximately equal to its free field power radiation. GMMA is able to predict the level of the sound power accurately everywhere while CMA fails.

### B. Direct field and reverberant field

The concepts of the direct field and the reverberant field have long been accepted by acousticians. An expression for the time averaged sound pressure in terms of the direct sound pressure and the reverberant sound pressure has been obtained based on the energy diffusion equation as[15]

$$p^2 = \Pi \rho_0 c \left[ \frac{1}{4\pi r_d^2} + \frac{4(1 - \alpha_e)}{S \alpha_e} \right], \tag{22}$$

where $\Pi$ is the source power, $S$ is the inner surface area of the room, $r_d$ stands for the distance from the point source to the field point, and $\alpha_e$ is the effective absorption coefficient. The first term on the right hand side of Eq. (22) represents the direct field and the second term represents the reverberant field. The critical distance is defined by the distance from the source to where the direct sound pressure is equal to the reverberant sound pressure and can be computed by the following formula:

$$R_c = \sqrt{\frac{S \alpha_e}{16\pi(1 - \alpha_e)}}. \tag{23}$$

There has been much discussion on how to best compute the effective absorption coefficient, $\alpha_e$.[16–22] In this example, the effective absorption coefficient of a room will be computed numerically based on GMMA, and compared to the results of some existing formulas. Dimensions of the room under test are $\sqrt{15} \times \pi \times 5$ m³. Different boundary conditions are implemented, and the Sabine absorption coefficient varies from 0.05 to 0.8. The Schroeder frequency for these conditions varies from 447 to 100 Hz. Five frequencies in the
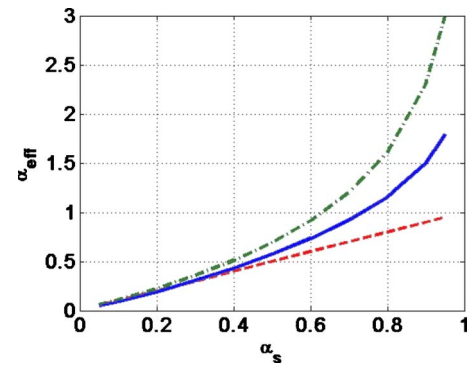


FIG. 9. (Color online) Effective absorption coefficient as a function of Sabine's absorption coefficient calculated in a rectangular room for the 630 Hz one-third octave band. "—:" GMMA prediction; "– –:" Sabine's formula; "–·–:" Eyring's formula.

630 Hz one-third octave band were chosen to drive a point source. Sound fields are computed ten times at each frequency with the source location randomly chosen each time. The averaged critical distances calculated directly from the direct field and reverberant field results are used to calculate the effective absorption coefficient using Eq. (23). Figure 9 compares the numerical results with Sabine's formula and Eyring's formula. The GMMA results (with around 1500 modes) generally fall in the middle of them, which is very similar to the results of Joyce[18] (the curve "$s = 7/9$" in his Fig. 4) and Jing et al.[22]

### C. Complex sources

In practice, sound sources are often complex extended sources, rather than point sources (monopoles). For a distributed source placed inside an enclosure, computation may be very difficult and time consuming with pure modal models; however, a simple modification of the hybrid modal expansion method can solve this problem easily for cases where the size of the source is small compared to the dimensions of the enclosure. If, for example, the free field directivity pattern, $D(r, \phi, \theta)$, of a distributed source is known, one can simply replace the free field Green's function ($G$) in Eqs. (13) and (15) with $D(r, \phi, \theta)$ and compute the sound field without much additional computation required. Figure 10 compares the pressure fields of two different sources placed in the "Damped enclosure 2" (see Table II) using the GMMA model with around 2000 modes. Two small sources are located at the center of the enclosure and both are driven at a frequency of 400 Hz. However, they have different free field directivity patterns: (1) an omnidirectional source $[D(r, \phi, \theta) = 1]$, (2) a complex source $[D(r, \phi, \theta) = \sqrt{2} \cos(\theta/2)]$. Pressure fields on the x-y, y-z and x-z planes that include the source are plotted. Effects of the source directivity are clearly represented by the GMMA model.

The closed form expression of the free field response of a source is usually not available, but if the multipole expansion is known, the hybrid modal expansion can be certainly implemented straightforwardly and Eqs. (13) and (15) can be modified to

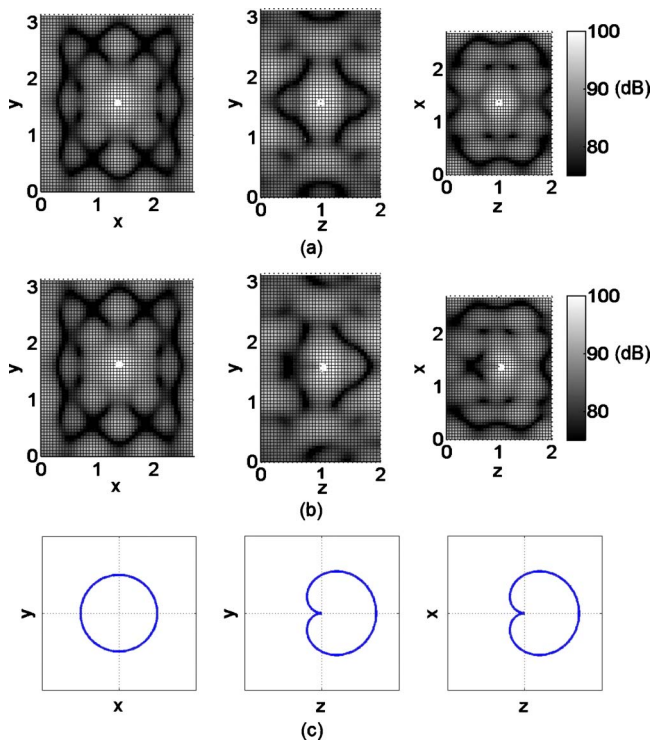$$\hat{p}(\mathbf{r}) = \hat{p}_0 + F(\mathbf{r}) \tag{24}$$

FIG. 10. (Color online) Sound pressure level computed by GMMA for (a) a monopole source and (b) a small complex source in a rectangular room (damped room 2) at 400 Hz. Both sources are placed at the center of the room. Pressure fields on the x-y, y-z and x-z planes that include the source are plotted with the white dots representing the location of the sources. The directivity pattern of the small complex source is shown in (c).

and

$$\sum_n \left[ (k_0^2 - k_m^2) C_{mn} + D_{mn} \right] q_n$$

$$= - \oint_S \psi_m^* \left( \beta \hat{p}_0 - \frac{\partial \hat{p}_0}{\partial \mathbf{n}} \right) da$$

$$= - \sum_{m=1}^M A_m \oint_S \psi_m^* \left( \beta \Phi_m - \frac{\partial \Phi_m}{\partial \mathbf{n}} \right) da, \qquad (25)$$

where $\hat{p}_0 = \sum_{m=1}^M A_m \Phi_m$, the multipole expansion for the free field sound pressure of a complex source, and $\Phi_m$ represents the expression of the $mth$ multipole and $A_m$ stands for the amplitude of that multipole.

## V. CONCLUSIONS

Different modal expansion methods have been studied in this paper. A set of modified modes are introduced to deal with damped enclosures. A free field Green's function is integrated to the solution of the non-homogeneous Helmholtz equation to improve both convergence rate and accuracy of modal expansions.

Like the normal modes, the modified modes are complete and orthogonal. For damped boundary conditions, the modified modes are mutually coupled, which causes the computation time to increase significantly, as is the case for the normal modes. However, by partially satisfying the boundary conditions, MMA not only performs better than CMA in the region near boundaries but also is more accurate

globally with even fewer modes used. In addition, the "uncoupled" MMA can predict sound pressure level and particle velocity level fairly accurately for many damped boundary conditions, while the "uncoupled" CMA usually introduces large errors. Usually, MMA requires numerically searching for the eigenvalues. This process is fairly straightforward and fast. Utilizing the univariate interval Newton/generalized bisection method,[6] it took less than 1 s to calculate 20 000 eigenvalues for any of the rooms listed in Table II on a computer with a 2.1 GHz CPU.

The enclosed sound field can be separated into the direct field and reverberant field, but these two are treated together in the traditional modal analysis. The weaknesses include slow convergence rate (especially in the near field of a point source) and difficulty in dealing with complicated sources inside an enclosure. The hybrid modal expansion introduced in this paper successfully addresses these problems. Studies on a point source in rectangular enclosures show that the hybrid modal expansions converge notably faster than the regular modal expansions and the hybrid "uncoupled" modal expansions introduce much smaller errors than the regular "uncoupled" expansions. The hybrid modal expansion can be easily applied to complex sound sources if the free field responses of the sources are known.

[1] P. M. Morse and R. H. Bolt, "Sound waves in rooms," Rev. Mod. Phys. **16**, 69–150 (1944).

[2] E. H. Dowell, G. F. Gorman, and D. A. Smith, "Acoustoelasticity: General theory, acoustic natural modes and forced response to sinusoidal excitation, including comparisons with experiment," J. Sound Vib. **52**, 519–542 (1977).

[3] L. P. Franzoni and E. H. Dowell, "On the accuracy of modal-analysis in reverberant acoustical systems with damping," J. Acoust. Soc. Am. **97**, 687–690 (1995).

[4] G. B. Arfken and H.-J. Weber, *Mathematical Methods for Physicists*, 5th ed. (Harcourt/Academic, San Diego, 2001), pp. 893–897.

[5] S. R. Bistafa and J. W. Morrissey, "Numerical solutions of the acoustic eigenvalue equation in the rectangular room with arbitrary (uniform) wall impedances," J. Sound Vib. **263**, 205–218 (2003).

[6] Y. Naka, A. A. Oberai, and B. G. Shinn-Cunningham, "Acoustic eigenvalues of rectangular rooms with arbitrary wall impedances using the interval Newton/generalized bisection method," J. Acoust. Soc. Am. **118**, 3662–3671 (2005).

[7] D.-Y. Maa, "Sound field in a room and its active noise control," Appl. Acoust. **41**, 113–126 (1994).

[8] D.-Y. Maa, "Formula of sound field in a room, re-examination," Acta Acust. (Beijing) **27**, 385–388 (2002).

[9] G. B. Arfken and H.-J. Weber, *Mathematical Methods for Physicists*, 5th ed. (Harcourt/Academic, San Diego, 2001), Chap. 9.

[10] J. Pan, "A second note on the prediction of sound intensity," J. Acoust. Soc. Am. **97**, 691–694 (1995).

[11] M. P. Morse, "The transmission of sound inside pipes," J. Acoust. Soc. Am. **11**, 205–210 (1939).

[12] A. D. Pierce, *Acoustics: An Introduction to Its Physical Principles and Applications*, McGraw-Hill Series in Mechanical Engineering (McGraw-Hill, New York, 1981), Chap. 3.

[13] L. E. Kinsler, *Fundamentals of Acoustics*, 4th ed. (Wiley, New York, 2000), Chap. 9.

[14] J. Pan, "A note on the prediction of sound intensity," J. Acoust. Soc. Am. **93**, 1641–1644 (1993).

[15] L. L. Beranek, *Acoustics* (McGraw-Hill, New York, 1954), Chap. 10.

[16]W. C. Sabine, *Collected Papers on Acoustics* (Dover, New York, 1964), Chap. 1.

[17]C. F. Eyring, "Reverberation Time in 'Dead' Rooms," J. Acoust. Soc. Am. **1**, 168 (1930).

[18]W. B. Joyce, "Exact effect of surface roughness on the reverberation time of a uniformly absorbing spherical enclosure," J. Acoust. Soc. Am. **64**, 1429–1436 (1978).

[19]W. B. Joyce, "Power series for the reverberation time," J. Acoust. Soc. Am. **67**, 564–571 (1980).

[20]M. Hodgson, "Experimental evaluation of the accuracy of the Sabine and Eyring theories in the case of non-low surface absorption," J. Acoust. Soc. Am. **94**, 835–840 (1993).

[21]L. L. Beranek, "Analysis of Sabine and Eyring equations and their application to concert hall audience and chair absorption," J. Acoust. Soc. Am. **120**, 1399–1410 (2006).

[22]Y. Jing and N. Xiang, "On boundary conditions for the diffusion equation in room acoustic prediction: Theory, simulations, and experiments," J. Acoust. Soc. Am. **123**, 145–153 (2008).